Citation: Lixia Wang, Zilin Hu, Qing Wang, et al. Study on pressure-sensitive properties of carbon fiber powder reinforced lime-improved silty sand. *Journal of Harbin Institute of Technology (New Series)*. DOI: 10.11916/j.issn.1005-9113.24006

Study on Pressure-Sensitive Properties of Carbon Fiber Powder Reinforced Lime-Improved Silty Sand

*Lixia Wang, Zilin Hu, Qing Wang and Yunlong Zhang**

(*School of Transportation Science and Engineering, Jilin Jianzhu University, Changchun 130119, China*)

Abstract: This study tested the electrical conductivity and pressure sensitivity of lime-improved silty sand reinforced with Carbon Fiber Powder (CFP) as the conductive medium. The influence of CFP dosage, moisture content and curing duration on the unconfined compressive strength, initial resistivity and pressure sensitivity of the improved soil was systematically analysed. The results showed that the unconfined compressive strength varied non-monotonically with increasing CFP dosage, reaching a peak at a dosage of 1.6%. Furthermore, the initial resistivity showed slight variations under different moisture conditions but eventually converged towards the conductive percolation threshold at a dosage of 2.4%. It is worth noting that CFP reinforced lime-improved silty sand (CRLS) exhibit a clear dynamic synchronization of strain with stress and resistivity rate of variation. The pressure sensitivity was optimized with CFP dosages ranging from 1.6% to 2.0%. Both insufficient and excessive dosages had a negative impact on pressure sensitivity. It is important to consider the weakening effect of high moisture content on the pressure sensitivity of the specimens in practical applications.

Keywords: lime-improved silty sand; CFP; unconfined compressive strength; resistivity; pressure-sensitivity

CLC number: TU521 **Document code**: A **Article ID**: 1005-9113(2024)00-0000-10

0 Introduction

Lime-improved soil has better strength, environmental performance and more economic benefits compared with cement-amended soil[1-2], so it is widely used in highway construction. The evaluation of roadbed soil engineering characteristics and monitoring of road operating conditions are crucial with the continuous increase in China's highway and infrastructure construction. It is important to ensure convenient and efficient methods for carrying out these tasks.

In the 1995, Chung[3] first proposed self-sensing concrete. Since then, many researchers in academia have conducted extensive research on this topic. Functional fillers, such as carbon nanotubes[4], carbon fibers[3-6] and carbon black[4,7], can be added to the concrete matrix to give it self-aware properties. This increases the material's durability and mechanical qualities while also making it more sensitive to pressure. As a result, it can be used as a sensor for the identification of structural damage, which has reference significance for the study of soil pressure sensitivity. Fu et al.[8] discovered through uniaxial compression synchronous resistivity tests that the dynamic changes in stress-strain-resistivity during compression in frozen soil exhibit synchronization. At various damage levels, Wang et al.[9] focused on the connection between damage variable and rock resistivity. The link between resistivity and elastic modulus during rock deterioration served as the foundation for their development of the variation law. Jia et al.[10] found that the rate of resistivity variation during the initial compaction stage of sandstone could reflect the initial damage degree of rocks through the uniaxial compression synchronous resistivity test of sandstone with different high-temperature damages. Zhou et al.[11] found that the resistivity of loess was more sensitive to loading effects at loads below 200 kPa. Chen et al.[12] studied the uniaxial compression process of red clay that underwent dry-wet cyclic action, and found that the dry-wet cyclic

Received 2024-01-26

Sponsored by Jilin Provincial Department of Education Scientific Research Project (JJKH20190875KJ) and (JJKH20230348KJ)

* Corresponding author: Yunlong Zhang, Ph.D, Professor. E-mail: zhangyunlong@jlju.edu.cn.

action had little effect on the pattern of change in its resistivity-stress-strain curve. Dong et al.[13] showed on unsaturated loess that the pore water channels inside the specimen changed under loading, and the changes in porosity and current paths had a large effect on the resistivity. An et al.[14] formulated a resistivity-based damage model for residual soil subjected to uniaxial loading, utilizing resistivity test data as the foundation for their analysis.

In addition, numerous scholars have extensively researched the pressure sensitivity of improved soils. Salih et al.[15] investigated the resistivity-strain relationship of desulfurized gypsum-fly ash modified red mud under different moisture content and different dry-wet cycles, they found a linear relationship between resistivity and strain within the elastic phase of the specimens, indicating a strong pressure sensitivity. Wang et al.[16] discovered that the curing age of red mud modified lime soil had little effect on the stress-strain-resistivity change pattern. The change pattern remained consistent under consistent red mud content. Shen[17] incorporated copper ions into red mud solidified soil, revealing that moderate copper content enhances pressure sensitivity, whereas excessive levels attenuate it. Ma et al.[18] analyzed the dynamic resistivity characteristics of solidified cadmium contaminated soil and established its dynamic resistivity model. Wen et al.[19] investigated cemented soils composed of red mud and calcium and found that its pressure sensitivity gradually weakened with the freeze-thaw cycle. The alterations in resistivity and pressure sensitivity effectively characterized freeze-thaw-induced damage. Song et al.[20] found that zinc-contaminated red clay has good pressure sensitivity under different zinc contents, accurately reflecting changes in strength under loading. Ban et al.[21] treated red clay with carbonated reactive MgO and derived a correlation between strength and resistivity through simultaneous unconfined compression and resistivity testing. This correlation provides a predictive tool for evaluating the resistivity and strength characteristics of carbonated red clay. The above studies have used chemical reagents to improve the soil, which will have a certain impact on the environment.

Short carbon fiber is widely used in intelligent concrete structures due to its excellent electrical conductivity. The incorporation of carbon fibers effectively augments the electrical conductivity of the cement matrix through tunnel conductive effect and conductive percolation[22], such as strain sensing, piezoresistive effect, which have been used as sensors in the field of structural health monitoring and achieved significant results[23]. Because carbon fiber is easy to agglomerate when mixing with soil, which affects the strength and electrical stability of soil, Li et al.[24] used CFP, which has fine shape and is easily dispersed, to enhance cement mortar. They investigated the piezoresistive characteristics of carbon fiber powder at dosages of 2%, 4%, and 6%.

In summary, CFP was used as the conductive medium in this study. The influence laws and change mechanisms of CFP content, moisture content and curing duration on the unconfined compressive strength, initial resistivity and pressure sensitivity of CRLS were investigated and analyzed. The optimum content of CFP was determined, which provided experimental reference for the research and promotion of intelligent road materials.

1 Materials and Methods

1.1 Test Materials

The soil used in the experiment is made up of silty sand that comes from a construction site in Songyuan, in the province of Jilin. The fundamental physical characteristics are presented in Table 1, while the outcomes of the particle analysis test are detailed in Table 2. The high-purity quicklime powder with calcium content of 99% was used in the test, which met the requirements of Test Methods of Materials Stabilized with Inorganic Binders for Highway Engineering (JTG E51-2019). The parameters of purchased CFP materials are shown in Table 3.

Table 1 Basic physical properties of silty sand

Maximum dry density ($g \cdot cm^{-3}$)	Optimal moisture content (%)	Liquid limit (%)	Plastic limit (%)	Plasticity index
1.84	9.7	21.5	14.1	7.4

Table 2 Test results of particle analysis of silty sand

Particle size (mm)	2.000	1.000	0.500	0.250	0.075	0.010	0.005
Percentage of total soil mass represented by soil particles smaller than that size(%)	99.97	96.39	81.58	60.60	10.89	3.56	1.05

Table 3 CFP material parameters

Mesh	Carbon content (%)	Monofilament diameter (mm)	Tensile strength(MPa)	Resistivity(Ω·m)
50	>95	7	≥3500	14×10^{-6}

1.2 Preparation of Test Specimens and Experimental Arrangements

The silty sand was crushed and passed through 2 mm sieve, then sealed and preserved by oven drying. Based on the engineering experience, the lime mixing amount of soil for specimens was set at 8% of the dry soil mass, and the CFP content was 0.4%, 0.8%,1.2%, 1.6%, 2.0%, 2.4%, 3.0%, 4.0 % of the total mass of the lime soil, respectively. The specimens were prepared by mixing dry soil, quicklime and CFP. The optimal moisture content for lime soil was found to be 15.0% according to the compaction test method of inorganic binder stabilized soil (JTG E51-2019) before specimen preparation. To control the influence of water on the test, the specimens were configured with three different moisture contents of 13 %, 15 % and 17 % respectively. After full mixing, the cylindrical specimens with a diameter of 39.1 mm and a height of 80 mm were prepared in accordance with the test methods of soils for highway engineering (JTG3430-2020), and compacted with 100% compactness. Subsequently, the specimens were demolded, grouped and numbered and wrapped with plastic wrap before being placed in a standard constant temperature and humidity curing box with the temperature at 20 ℃ ± 2 ℃ and the humidity greater than 95 % to maintain 7 d,14 d and 28 d. The experimental arrangement is shown in Table 4.

Table 4 Experimental arrangements

Test category	Moisture content (%)	CFP dosage (%)	Maintenance time (d)
Unconfined compression test/ resistivity test/pressure sensitivity test	13.0	0.0,0.4,0.8,1.2,1.6,2.0,2.4,3.0,4.0	7,14,28
	15.0	0.0,0.4,0.8,1.2,1.6,2.0,2.4,3.0,4.0	7,14,28
	17.0	0.0,0.4,0.8,1.2,1.6,2.0,2.4,3.0,4.0	7,14,28

1.3 Resistivity Test and Pressure Sensitivity Test

After the specimen reached the corresponding maintenance age, the upper and lower surfaces of specimen were ground smooth, a layer of graphite powder was uniformly coated at both ends, and the specimen was clamped with a copper plate to ensure that it was in close contact with the specimen. This test was connected by two-phase electrode method, and the circuit diagram is depicted in Fig. 1, while equipment such as MS-155D DC voltage stabilized power supply and model VC890D multimeter were equipped for resistivity testing of soil specimens. The resistivity of the soil is determined using the following formula: $r = RS/L$, where r is the resistivity (Ω·m); R is the resistance (Ω); S is the transverse area of specimen (m^2); L is the length of specimen (m).

The pressure sensitivity test was carried out simultaneously with the resistivity test using the multi-functional servo dynamic and static triaxial test instrument produced by Wille company in Germany. The specimen underwent a test in which graphite powder was applied to its upper and lower surfaces and then clamped with copper. Insulating pads were also attached to the specimen's upper and lower extremities. To guarantee complete fitting of the copper sheet and insulation block on the upper and lower surfaces of the specimen, a contact stress of 35 kPa was set before pressing. The test method adopted the vertical strain control method without peripheral pressure, loading vertically at a rate of 0.8 mm/min, and recording the numerical changes of stress, strain and resistivity synchronously throughout the loading process. The pressure sensitivity test equipment is presented in Fig.2.

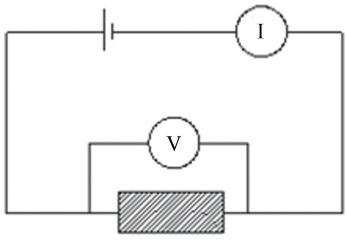

Fig.1 Resistivity test circuit diagram

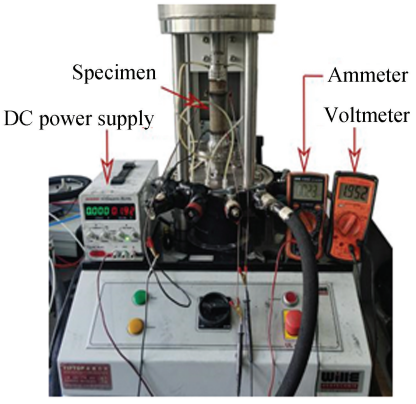

Fig. 2 Pressure sensitivity test equipment

2 Results and Discussion

2.1 Strength Analysis

To delve into the impact of CFP content on the unconfined compressive strength of CRLS, Fig. 3 illustrates the correlation between the specimens' unconfined compressive strength and CFP content, taking into account varying moisture levels and curing durations.

Fig.3 illustrates that the unconfined compressive strength of the specimens gradually enhances with the accumulation of curing duration, peaking at 28 d. Under constant moisture content conditions, the unconfined compressive strength of specimen exhibits a wavy pattern with increasing CFP content, initially decreasing, then peaking at an optimal dosage, and subsequently decreasing and stabilizing. The change characteristics of the three stages are basically presented: The low content stage displays a descending trend, the moderate content stage exhibits an ascending trend, and the high content stage indicates a downward and tends to stabilize the trend. Among them:

1) In the low content stage, under the condition of 13% or 15% moisture content and 0.4%−1.2% CFP content, the unconfined compressive strength of CRLS is inferior to that of pure lime soil. Under the condition of moisture content of 17% and CFP content of 0.4%, the unconfined compressive strength of CRLS is the lowest.

2) In the moderate content stage, with the gradual increase of CFP content, the unconfined compressive strength of the specimens began to increase. The maximum unconfined compressive strength is achieved when the moisture content is 13% and the CFP content is 2.0%, or when the moisture content is 15% or 17% and the CFP content is 1.6%. The corresponding strengths are 207.3 kPa, 181.9 kPa and 200.1 kPa, respectively. The addition of CFP has increased the unconfined compressive strength by 1.64, 1.28, and 1.59 times compared to specimens without CFP.

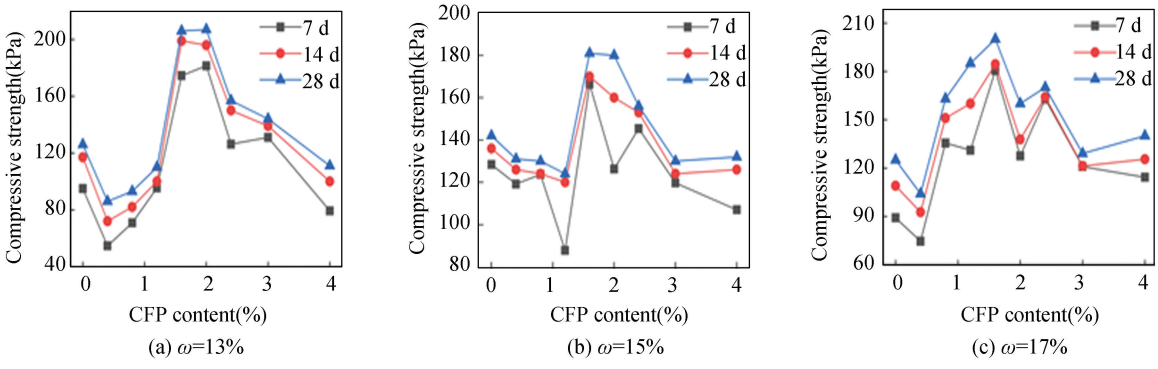

Fig.3 Relationship curve between unconfined compressive strength and CFP content

3) In the high content stage, the unconfined compressive strength of the specimen experiences a steady decline as the CFP content rises. The strength gradually tends to stabilize when the content exceeds 3.0%.

Under varying dosage conditions, the impact of CFP on CRLS exhibits different patterns and mechanisms of change. At low dosages, CFP does not

adequately fill the soil pores, resulting in a reduction in strength due to decreased interparticle friction resistance. Under appropriate doping conditions, CFP and soil particles combine to form a particle-fiber unit. CFP act as a lap between the particles, effectively linking the soil particles. This enhances the integrity and strength of the soil body through the formation of particle-fiber units and fiber lap joints. However, under high dosage conditions, soil particles may not fully combine with excess CFP. The excess fiber will be free between the pores of the soil specimens, resulting in contact between the fibers and forming a lubricating effect. Additionally, the fiber surface will adsorb more water, which can affect the hydration behavior of lime and ultimately reduce the strength of the specimen. Therefore, controlling the dosage of CFP is crucial for bolstering the mechanical characteristics of CRLS.

In summary, the incorporation of appropriate amount of CFP can effectively improve the unconfined compressive strength of CRLS, and the optimum content of CFP is about 1.6%.

2.2 Initial Resistivity Analysis

In order to investigate the relationship between the content of CFP and the initial resistivity of lime-improved silty sand, the relationship between the initial resistivity of the specimen and the content of CFP under different moisture content and different curing age conditions are plotted in Fig.4.

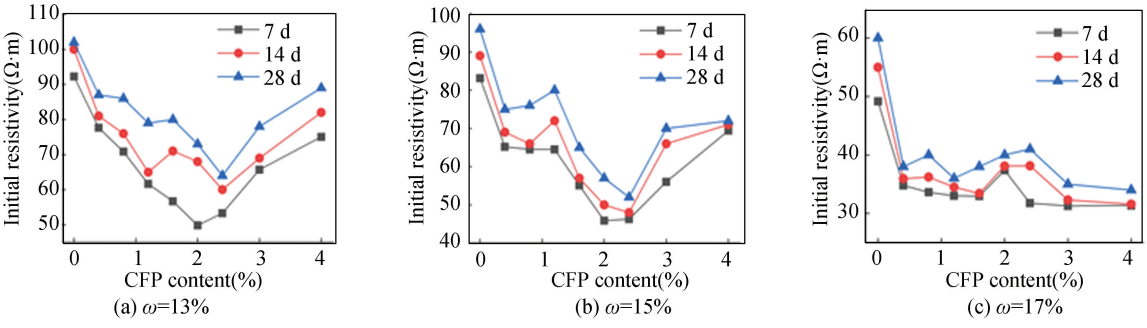

Fig.4 Relationship between initial resistivity and CFP content

Observing Fig. 4, one can discern that the initial resistivity of the specimens increases with the accumulation of curing duration, and reaches the maximum when the curing duration is 28 d. Under different moisture content conditions, the initial resistivity of the specimen without CFP is the largest, and its initial resistivity shows different trends with the increase of CFP content. The different moisture content can be divided into two cases for discusson: moisture content $w \leqslant 15\%$ and moisture content $w > 15\%$.

The analysis of Fig.4(a) and (b) reveals that under the condition of moisture content $w \leqslant 15\%$, the initial resistivity of the specimen shows a decreasing and then increasing trend with the enhancement of CFP content. When the content of CFP is increased to 2.4%, the initial resistivity of the specimen reaches the minimum value, and its minimum value of the initial resistivity is 64.61Ω · m when the moisture content is 13%, and the initial resistivity of CRLS is 37.0% lower than the initial resistivity of pure lime soil. When the moisture content is 15%, the minimum value of the initial resistivity is 52.11 Ω · m, the initial resistivity of CRLS compared to the initial resistivity of pure lime soil decreased by 45.8%. When the dosage of CFP exceeded 2.4%, the initial resistivity of the specimens increased. However, the increase was slowed down with the increase in CFP dosage. This phenomenon is attributed to excess CFP agglomeration, which creates a poor overlap between fibers. This in turn inhibits the formation of conductive circuits, leading to an increase in soil resistivity. The phenomena observed above are consistent with percolation[25-27]. The soil resistivity undergoes an abrupt change when the doping concentration reaches a certain critical value. Additionally, it indicates that a CFP doping level of 2.4% is near the percolation threshold. This is significant for optimizing the soil's electrical conductivity.

As can be seen from Fig. 4(c), under the condition of moisture content $w > 15\%$, the initial resistivity of the specimen exhibits a minor decreasing trend overall with a sustained increment in CFP content, but the initial resistivity of the specimen rises

slightly with the content of CFP in the interval of 1.6%-2.4%. As the CFP content surpasses 2.4%, the initial resistivity gradually decreases and ultimately tends towards stabilization. This behaviour can be ascribed to the increased connectivity of the pore water in specimens at high moisture contents, which creates a large number of conductive paths, leading to preferential propagation of electric current through the pore water. Therefore, moisture content is significant factor that determines the magnitude of the initial resistivity.

2.3 Pressure Sensitivity Analysis

2.3.1 *Relationship between stress, resistivity variation rate and strain*

To investigate the rules governing the resistivity variation rate of the specimen during loading, Fig.5 displays stress, resistivity variation rate, and strain curves of specimens with different maintenance ages under the condition of 1.6% CFP content and 15% optimal moisture content. The resistivity variation rate is $\Delta\rho/\rho_0(\%)$, of which $\Delta\rho$ is the difference of resistivity ($\Omega \cdot m$), $\Delta\rho = \rho - \rho_0$; ρ is the instantaneous resistivity ($\Omega \cdot m$); ρ_0 is the initial resistivity ($\Omega \cdot m$).

As can be seen from Fig.5, CRLS in uniaxial compression process of stress, resistivity variation rate and the dynamic change between the strain has significant synchronization. The resistivity variation rate can directly reflect the stress state of the specimen, and the rule of change can be roughly divided into three phases for discussion:

Stage Ⅰ: When the strain is small, the specimen is in the elastic compression stage, the stress increases linearly with the strain, and the resistivity variation rate decreases linearly with the strain. The compression of internal pores in the specimen narrows the conductive pathway and can connect previously unconnected pore water pathways. Additionally, compression narrows the spacing between the CFP, promoting the establishment of additional conductive pathways. As a result, the resistivity variation rate decreases rapidly during the early stage of compression.

Stage Ⅱ: As strain increases, the specimen enters the plastic deformation stage, and small cracks begin to appear. The stress with the increase of strain shows a nonlinear trend of increase, the resistivity variation rate with the increase of strain shows a nonlinear trend of decrease. The specimen stress and resistivity variation rate both reach the extreme values almost simultaneously. Furthermore, as the strain increases, the fine cracks that have developed within the specimen continue to grow and expand until they are completely penetrated.

Stage Ⅲ: As the strain continues to increase, the specimen enters the destruction stage, characterized by a sharp decrease in stress as strain builds up, ultimately resulting in the complete failure of the specimen. At this stage, the cracks on the surface of the specimen undergo rapid development, from the original tiny cracks to large cracks through the upper and lower surfaces of the specimen, while the resistivity variation rate of the specimen also increased rapidly.

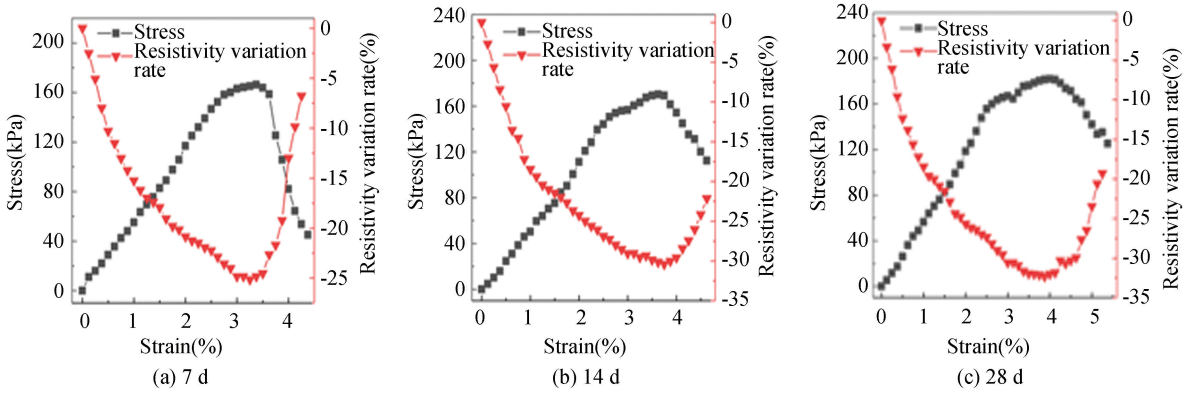

Fig.5 Relationship curves between stress, resistivity variation rate and strain in soil specimen

Fig. 6 illustrates the curves depicting the relationship between the resistivity variation rate and strain of CRLS at different curing duration under the condition of 1.6% CFP dosing.

It is evident that the resistivity variation rate of the specimen with a maintenance age of 7 d is small. As the curing duration reaches 14 d, the resistivity variation rate gradually increases, demonstrating that

the strength is forming and the internal structure is becoming more stable. For specimens with a curing duration of 14 d and 28 d, there were only minor differences in the curves that show the relationship between the resistivity variation rate and strain. At 28 d of curing duration, the resistivity variation rate of the specimen reaches 32.32%.

At the start of the conservation period, the degree of internal hydration is low, resulting in more pore water pathways. As a result, the compression process of the conductive pathway change is not significant, and the rate of resistivity variation is limited. After a certain period of curing, the hydration degree inside the specimen can be continuously enhanced, leading to a reduction in the number of conductive pathways in the pore water. This results in the initial resistivity of the specimen showing a high level. During the loading process, the specimen develops fine cracks internally and undergoes corresponding changes in microstructure, resulting in the formation of new pores. These newly formed pores increase the conductive path of pore water, leading to a significant reduction in the rate of variation of electrical resistivity. Therefore, the magnitude of this variation is particularly significant.

In summary, the pressure-sensitive properties of the specimens gradually stabilized after 28 d of curing as the curing time progresses. The resistivity variation rate of the specimen showed a more obvious decreasing trend during this process, resulting in more excellent pressure-sensitive performance.

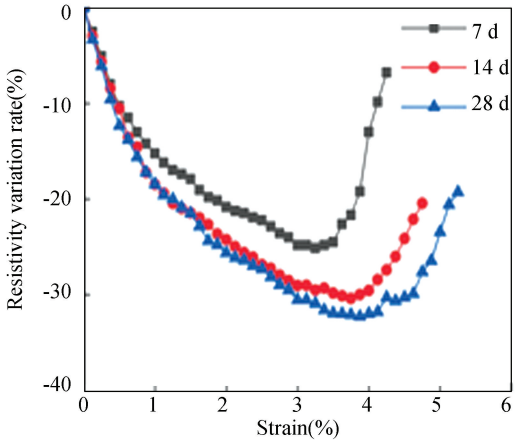

Fig. 6 Relationship curve between resistivity variation rate and strain of soil specimens at different ages

2.3.2 *Relationship between pressure sensitivity and CFP content*

In order to further explore the pressure sensitive performance of CRLS, the specimens cured for 28 d are selected as the focus of investigation, and the resistivity variation rate with strain under different CFP content and different moisture content conditions are plotted in Fig.7.

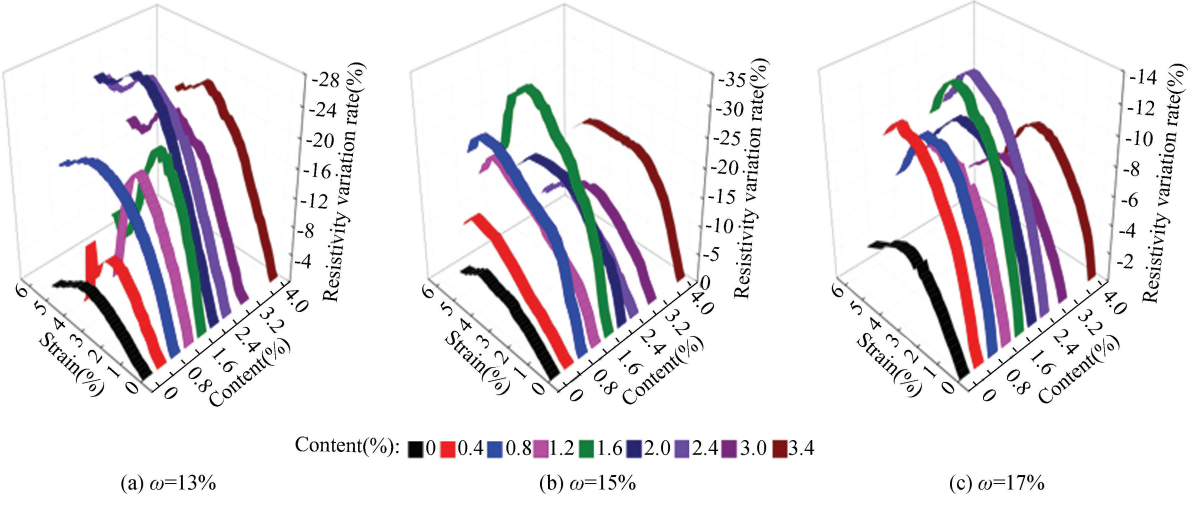

Fig.7 Band plot of resistivity rate of variation versus strain for soil specimens

As shown in Fig.7, the resistivity variation rate of the specimen decreases and then increases as the strain increases. During the initial stage of strain augmentation, the resistivity variation rate decreases linearly. In the middle stage, the decrease in resistivity variation rate slows down. In the late stage, the resistivity variation rate increases rapidly after reaching its minimum value, while the stress reaches

its peak.

It can also be seen from Fig.7 that the magnitude of reduction in the specimen's resistivity variation rate augments with an increment in the CFP content. When the CFP content is 0%, the degree of variation in specimen resistivity is at a minimum, the maximum resistivity variation rate is less than 8%. At lower CFP content (0.4%-1.2%), the specimens' resistivity alteration rate gradually increases as the content rises, albeit with varying degrees of decrement across different ratios. Moreover; When the CFP content reaches 1.6%-2.0%, the maximum resistivity variation rate of the specimen experiences a significant increase, signifying a notable improvement in its pressure sensitivity, especially when the content is 1.6%, the maximum resistivity variation rate of the specimen can reach 32.32%. However, once the proportion of CFP exceeds 2.4%, the resistivity variation rate of the specimen gradually diminishes, indicating that the improvement effect of its pressure sensitivity gradually weakens.

Combined with the previous analysis in Section 2.1, when the CFP is in small quantity, it fails to fully fill the pores and is not evenly distributed within the matrix, leading to unstable conductive pathways within the test piece and significant differences in pressure sensitivity. When the content amount reaches 1.6%, the CFP can effectively reduce the spacing between conductive particles by filling the pores between soil particles. This leads to a decrease in the potential barrier within the matrix and an increase in the probability of tunneling conductive effect and conductive percolation[17,22]. As a result, the rate of resistivity variation decreases more significantly, leading to an improvement in pressure sensitivity. When the content of CFP is excessive, the distribution of CFP in the soil becomes denser, resulting in excessive overlap. This causes the conduction of electrons and holes between the fibers to be mainly dominated by ohmic contacts rather than the tunneling effect. The alteration in conduction mode leads to a reduction in the significance of the resistivity alteration of CRLS when subjected to external pressure, thereby weakening its pressure-sensitive properties.

2.3.3 *Relationship between pressure sensitivity and moisture content*

The sensitivity coefficient is introduced as an indicator for analyzing the pressure sensitivity of soil specimens[28], with the following formula:

$$K = \frac{\Delta\rho/\rho_0}{\Delta\varepsilon}$$

In the formula, $\Delta\rho = \rho - \rho_0$, where $\Delta\rho$ is the resistivity difference ($\Omega \cdot m$); ρ is instantaneous resistivity ($\Omega \cdot m$); ρ_0 is the initial resistivity ($\Omega \cdot m$). $\Delta\varepsilon = \varepsilon_i - \varepsilon_{i-1}$, ε_i is the strain at any time.

The sensitivity coefficient in this paper is calculated by the data of the linear elastic stage during the compression process of the specimen. The relationship between the sensitivity coefficient of the soil specimen and the content of CFP under different moisture content conditions is plotted in Fig.8.

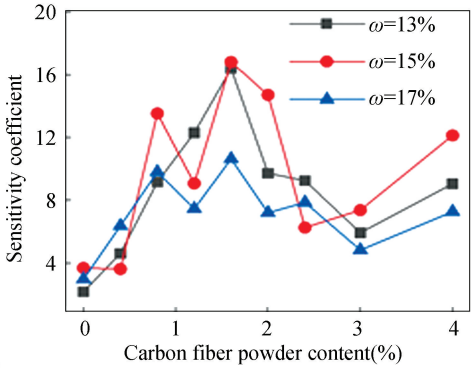

Fig. 8 Relationship between sensitivity coefficient and CFP content

As shown in Fig.8, under the three moisture content conditions, the specimens with 1.6% CFP content exhibit the maximum sensitivity coefficient, and the maximum sensitivity coefficients for the specimens with moisture contents of 13%, 15%, and 17% are 16.40, 16.81, and 10.64, respectively. Combined with Fig.7, it is evident that the specimen's resistivity variation degree exhibits the least diminution under 17% moisture content, peaking at 13.77%. In contrast, under 13% moisture content, the specimen attains a maximum resistivity variation degree of 26.75%. Notably, the degree of resistivity variation reaches its highest point at a moisture content of 15%, with a decrease of up to 32.32%.

In summary, the pressure sensitivity of the specimen is significantly affected by its moisture content. When the moisture content is low, more water is involved in the chemical reaction of lime, leading to less pore water, so the change in resistivity during compression is primarily due to the formation of tunnel conduction and conductive percolation between CFP. When the moisture content is high,

pore water and CFP collaborate to create numerous conductive pathways, resulting in an inherently low resistivity due to these pre-existing pathways. The additional conductive pathways formed during compression are limited, which limits the decrease in resistivity and results in a modest change in pressure sensitivity. Therefore, the moisture content should not be too high in the technical application.

3 Conclusions and Perspectives

1) The impact of CFP on the unconfined compressive strength of CRLS showed a wavy variation. As the CFP dosage increases, the strength initially decreases and then increases, reaching the peak strength at 1.6% doping and then gradually decreasing. The optimal unconfined compressive strength is achieved at a CFP content of approximately 1.6%.

2) The initial resistivity of CRLS under different moisture content conditions is slightly different with the increase of CFP. When the moisture content reaches the optimal level or is 2% below the optimal moisture content, the initial resistivity of the specimens exhibits a trend of decreasing followed by an increase as the CFP dosage increases. In particular, the resistivity approaches the percolation threshold at a dosage of 2.4%; whereas, when the moisture content exceeds the optimal level by 2%, the initial resistivity of the specimens demonstrates an overall decreasing trend as the CFP dosage increases.

3) The dynamic changes in the stress and resistivity rate of change versus strain relationship curves of CRLS are significantly synchronized. With the increase of strain, the specimens experience three stages: elastic compression, plastic deformation, and failure, which correspond to the trends of linear decrease, nonlinear decrease, and nonlinear increase of the resistivity variation rate, respectively. The stress and resistivity variation rate of the specimen reach their extremes almost simultaneously. The maximum rate of resistivity variation in the specimen increased with the duration of maintenance and stabilised after 28 d.

4) With the increase of CFP content, the pressure sensitivity of CRLS gradually improved, but the pressure sensitivity of the specimen will be reduced when the CFP content is less or too high. The specimen has the optimal pressure sensitivity performance of the optimal CFP content of 1.6% – 2.0%. The high moisture content has a weakening effect on the pressure sensitivity of the specimen, which needs to be considered in practical applications.

5) Scholars globally have studied in-depth the vibration characteristics of pile foundations[29-31] as well as the mechanical response of roadbeds under traffic loads[32]. As a follow-up to this study, theoretical numerical models will be developed in combination with field tests to simulate and predict soil pressure sensitivity, to elucidate the mechanical behaviour and damage law of the soil, and to provide a theoretical basis for the safety assessment and long-term performance monitoring of engineering structures under vibration.

References

[1] Sas W, Głuchowski A, Margielski J. Estimation of physical and mechanical properties of cohesive soil stabilized by hydratized lime addition. Annals of Warsaw University of Life Sciences-SGGW Land Reclamation, 2013, 45(45): 143-157. DOI: 10.2478/sggw-2013-0012.

[2] Bozbey I, Kamal N A, Abut Y. Effects of soil pulverisation level and freeze and thaw cycles on fly-ash- and lime-stabilised high plasticity clay: Implications on pavement design and performance. Road Materials and Pavement Design, 2017, 18(5): 1098 – 1116. DOI: 10.1080/14680629.2016.1207553.

[3] Chung D D L. Strain sensors based on the electrical resistance change accompanying the reversible pull-out of conducting short fibers in a less conducting matrix. Smart Materials and Structures, 1995, 4(1): 59 – 61. DOI: 10.1088/0964-1726/4/1/009.

[4] Al-Dahawi A, Yıldırım G, Öztürk O, et al. Assessment of self-sensing capability of engineered cementitious composites within the elastic and plastic ranges of cyclic flexural loading. Construction and Building Materials, 2017, 145: 1-10. DOI: 10.1016/j.conbuildmat.2017.03.236.

[5] Şahmaran M, Al-Dahawi A, Farzaneh V, et al. Self-sensing behavior under monotonic and cyclic loadings of ECC containing electrically conductive carbon-based materials. Proceedings of 3rd International Sustainable Buildings Symposium (ISBS 2017). Berlin: Springer, 2018: 566-576. DOI: 10.1007/978-3-319-64349-6_45.

[6] Xiao J, Grier A, Faustoferri R, et al. Association between oral candida and bacteriome in children with severe ECC. Journal of Dental Research, 2018, 97(13): 1468 – 1476. DOI: 10.1177/0022034518790941.

[7] Li M, Lin V, Lynch J P, et al. Carbon black engineered cementitious composites-mechanical and electrical characterization. SP-292: Structural Health Monitoring Technologies, 2013, 292: 1-16. DOI: 10.14359/51686287.

[8] Fu W, Wang R, Li Z, et al. Experimental study of electrical resistivity properties and alert performance of

frozen soil under uniaxial load. Rock and Soil Mechanics, 2009,30(7):1974-1980.
[9] Wang Y, Liu Y, Ma H. Changing regularity of rock damage variable and resistivity under loading condition. Safety Science, 2012, 50(4):718-722. DOI:10.1016/j.ssci.2011.08.046.
[10] Jia P, Li B, Zhu P, et al. Electrical response characteristics of high temperature damaged sandstones under uniaxial compression. Journal of Northeastern University (Natural Science), 2023,44(4): 558-564. DOI:10.12068/j.issn.1005-3026.2023.04.014.
[11] Zhou Y, Li G, Ma W, et al. Experimental study on electric resistivity characteristics of compacted loess under different loads and drying-wetting cycles. Advances in Civil Engineering, 2021, 2021(7): 1-12. DOI: 10.1155/2021/6672430.
[12] Chen Y, Huang X, Chen X, et al. Relationship between unconfined compressive strength and electrical resistivity of red clay under dry and wet cycles. Journal of Guangxi University (Natural Science Edition), 2020, 45(6): 1267-1275.
[13] Dong X, Huang F, Su N, et al. Experimental study of AC electrical resistivity of unsaturated loess during compression. Chinese Journal of Rock Mechanics and Engineering, 2015, 34(1): 189-197.
[14] An R, Kong L, Bai W, et al. The resistivity damage model of residual soil under uniaxial load and the law of drying-wetting effects. Chinese Journal of Rock Mechanics and Engineering, 2020, 39(S1): 3159-3167. DOI:10.13722/j.cnki.jrme.2019.0514.
[15] Salih W T, Yu W, Dong X, et al. Study on stress-strain-resistivity and microscopic mechanism of red mud waste modified by desulphurization gypsum-fly ash under drying-wetting cycles. Construction and Building Materials, 2020, 249(7): 118772. DOI: 10.1016/j.conbuildmat.2020.118772.
[16] Wang T, Hao Z, Yao X. Study on stress-strain-resistivity of lime soil modified by red mud. Bulletin of the Chinese Ceramic Society, 2019,38(5):1591-1596. (in Chinese)
[17] Shen K. Experimental study on pressure sensitive properties of copper contaminated soil solidified by modified red mud. Journal of Environmental Engineering and Landscape Management, 2019, 27(2): 93-100. DOI: 10.3846/jeelm.2019.9799.
[18] Ma Q, Zhang J, Cao J, et al. Mechanical characteristics of solidified chromium contaminated soil on the basis of resistivity representations. Journal of Taiyuan University of Technology, 2024, 55(5): 823-831. DOI: 10.16355/j.tyut.1007-9432.20220468.
[19] Wen H, Suo C, Hao Y, et al. Effect of freezing-thawing cycle on the mechanical properties and micromechanism of red mud-calcium-based composite cemented soil. Advances in Civil Engineering, 2020, 2020(1):825576. DOI: 10.1155/2020/8825576.
[20] Song Y, Gan X, Li H, et al. Curing effect and resistivity evolution of zinc-contaminated red clay cured by phosphate-based binder. Geofluids, 2022, 2022(1): 404620. DOI: 10.1155/2022/8404620.
[21] Ban R, Chen X, Yang X, et al. Strength and electrical resistivity characteristic of carbonating reactive MgO-mixed red clay under different water contents. Arabian Journal of Geosciences, 2022, 15:657. DOI: 10.1007/s12517-022-09937-z.
[22] Xie N, Shi X, Feng D, et al. Percolation backbone structure analysis in electrically conductive carbon fiber reinforced cement composites. Composites Part B: Engineering, 2012, 43(8):3270-3275. DOI:10.1016/j.compositesb.2012.02.032.
[23] Hui L, Ping J O. Smart concrete, sensors and self-sensing concrete structures. Key Engineering Materials, 2008, 400-402:69-80. DOI: 10.4028/www.scientific.net/KEM.400-402.69.
[24] Li S, Chen Y, Cuo Y, et al. Analysis of piezoresistance characteristics of cement mortar mixed with carbon fiber powder. Science Technology and Engineering, 2022, 22(20): 8828-8833.
[25] Rejon L, Rosas - Zavala A, Porcayo-Calderon J, et al. Percolation phenomena in carbon black-filled polymeric concrete. Polymer Engineering & Science, 2000, 40(9): 2101-2104. DOI: 10.1002/pen.11342.
[26] Allam H, Duplan F, Amziane S, et al. Carbon fibers' percolation in smart cementitious materials considering sand characteristics. Materials and Structures, 2023, 56: article number103. DOI:10.1617/s11527-023-02187-9.
[27] Chao H W, Lai Y Y, Chang T H. Percolation effect on the complex permittivities of polymer blends. Polymers, 2023, 15(18): 3751. DOI:10.3390/polym15183751.
[28] Cao Y, Xu J, Jiang L, et al. Fabrication and piezoresistivity of self-sensing Ni nanowire cement composites . Acta Materiae Compositae Sinica, 2018, 35(4):957-963. DOI: 10.13801/j.cnki.fhclxb.20170622.001.(in Chinese)
[29] Yang Z, Zou X, Chen S. A simplified approach to the monopile-friction wheel dynamic interaction in composite foundation. Ocean Engineering, 2024, 294: 116780. DOI:10.1016/j.oceaneng.2024.116780.
[30] Yang Y, Zou X, Chen S. Interaction model for horizontal dynamic response of monopile-friction wheel composite foundation in marine area. Computers and Geotechnics, 2024,166:105999. DOI:10.1016/j.compgeo.2023.105999.
[31] Wu W, Lu C, Chen L, et al. Horizontal vibration characteristics of pile groups in unsaturated soil considering coupled pile-pile interaction. Ocean Engineering, 2023, 281: 115000. DOI: 10.1016/j.oceaneng.2023.115000.
[32] Feng S, Lei H. A settlement prediction model considering tidal loading and traffic loading of soft soil subgrade. Computers and Geotechnics, 2022,144:104639. DOI:10.1016/j.compgeo.2022.104639.